Chemical Engineering Science: X 10 (2021) 100098

Contents lists available at ScienceDirect

Chemical Engineering Science: X

journal homepage: www.elsevier.com/locate/cesx

Novel evaluation method to determine the local mixing time distribution in stirred tank reactors

J. Fitschen [a,*], S. Hofmann [a], J. Wutz [b], A. v. Kameke [a], M. Hoffmann [a], T. Wucherpfennig [b], M. Schlüter [a]

[a] Institute of Multiphase Flows, Hamburg University of Technology, Germany
[b] Boehringer Ingelheim Pharma GmbH & Co. KG, Germany

ARTICLE INFO

Article history:
Received 21 July 2020
Received in revised form 8 March 2021
Accepted 18 March 2021

Keywords:
Local mixing time
Stirred tank reactor
Experimental and numerical results
Novel image analysis method
Micro, meso and macro mixing
Compartment visualization

ABSTRACT

Stirred tank reactors are frequently used for mixing as well as heat- and mass transfer processes in chemical and biochemical engineering due to their robust operation and extensive experiences in the past. However, for cell culture processes like mammalian cell expression systems, special requirements have to be met to ensure optimal cell growth and product quality. One of the most important requirements to ensure ideal transport processes is a proper mixing performance, characterized typically by the global mixing time $t_{mix,global}$ or the dimensionless global mixing time $t_{mix,global} \cdot n$. As an evaluation method for mixing time determination, the time is usually determined until a tracer signal (e.g. conductivity) has reached a constant value after a peak has been introduced (e.g. by adding a salt). A disadvantage of this method is, that the position of tracer feeding as well as the position of the probe significantly influences the detected mixing time. Further on, the global mixing time does not provide any information about the spatial and temporal "history" of the mixing process to identify areas that are mixed poorly or areas that form stable compartments. To overcome this disadvantage, a novel image analysis will be presented in this study for the detailed characterization of mixing processes by taking into account the history of mixing. The method is based on the experimental determination of the local mixing time distribution by using a multi-color change caused by a pH-change in a bromothymol blue solution. A 3 L transparent stirred tank reactor is used for the benchmark experiment. To demonstrate the suitability of the new characterization method for the validation of numerical simulations, a calculation with a commercial Lattice-Boltzmann approach (*M-Star CFD*) has been performed additionally and evaluated regarding mixing time distributions. The exemplary application of image analysis to a numerical mixing time simulation shows good agreement with the corresponding experiment. On the one hand, this shows that the method can also be interesting for numerical work, especially for experimental validation, and on the other hand, this allows much deeper insights into the mixing behavior compared to conventional mixing criteria. For example the new method enables the characterization of mixing on different scales as well as the identification of micro- and macroscopic flow structures. The strong influence of the acid to base ratio on mixing time experiments becomes clearly visible with the new method.

1. Introduction

In chemical and bioprocess engineering, mixing plays a key role, since it controls the process performance regarding solid suspension, homogenization, dispersion of multiple phases, heat transfer and chemical reactions. Rotating impellers create a turbulent flow, which leads to a variety of different mixing structures on different temporal and spatial scales. For a better understanding, one has to subdivide the mixing into a macro, meso and a micro scale contribution (Cheng et al., 2012; Zlokarnik, 2001; Sommer, 2010).

Basically, a convective turbulent transport in addition to chaotic flow and vortex motion on a macroscopic scale can be considered as macro mixing. The mixing process on the scale of single particles like bubbles or droplets down to the size of turbulent eddies is considered as meso mixing. Meso mixing can be found for example in the wake of particles. As soon as the scale of segregation is reduced to the Kolmogorov length scale, micro mixing proceeds by molecular diffusion, during which chemical reactions can occur (Bourne, 1983; Mao and Yang, 2017). Hence, the quality of mixing is defined by the knowledge about both independent values: the scale and intensity of segregation in a mixture (Danckwerts, 1952).

* Corresponding author.
E-mail address: juergen.fitschen@tuhh.de (J. Fitschen).
URL: http://www.tuhh.de/ims (J. Fitschen).

https://doi.org/10.1016/j.cesx.2021.100098
2590-1400/

Nomenclature

Symbols

c	concentration, mol l^{-1}
D	diffusion coefficient, m^2/s
D	tank diameter, m
d	stirrer diameter, m
H	filling height, m
I	light intensity, –
M	grade of homogeneity, –
n	stirrer frequency, rpm
P	power input, W
r_A	point of addition, m
s	stirrer clearance, m
$t_{mix,0.95}$	global mixing time, s
u	velocity, m s^{-1}
V	reactor volume, m^3
X	acid to base ratio, –
x	Lattice spacing, m

Dimensionless Numbers

Ba	Batchelor number, –
C	Courant number, –

Abbreviations

CHO	Chinese Hamster Ovary
PIV	Particle Image Velocimetry
pLIF	Planar laser-induced fluorescence

Sub- and Superscripts

A	point of addition, –
avg	average value, –
m	pixel row index, –
mix	mixing, –
n	pixel column index, –

In order to quantify the mixing efficiency, multiple measurement methods were discussed in the past decades, beginning with the basic classification and comparison of physical and chemical methods (Manna, 1997; Paul et al., 2004). Different physical measurement methods like temperature pulse (Rewatkar and Joshi, 1991; Hoogendoorn and den Hartog, 1967), electrical conductivity (Otomo et al., 2003; Buwa et al., 2006), electrochemical limiting current technique (Aydin and Yapici, 2018) or decolorization reactions with either iodine and sodium thiosulfate in water (Schaepe et al., 2013; Sieblist et al., 2011; Rodriguez et al., 2013) or acid-base neutralization reactions with phenolphthalein (Rice et al. (1964), Cabaret et al. (2007), Fox and Gex (1956)) or bromothymol blue (Lamberto et al., 1996; Cabaret et al., 2007) were widely used to determine the mixing time. In most cases, however, only the global mixing time $t_{\mathrm{mix,global}}$ is determined (Zlokarnik, 2001), which leads to an overall value for the respective discontinuous mixing process regarding its homogeneity. However, a spatial visualization of the local mixing time has only been carried out in shaken bioreactors by means of a neutralization reaction (Rodriguez et al., 2013; Rodriguez et al., 2018).

Mixing performance in stirred tanks has been investigated experimentally in various studies over the past years, but also a large number of numerical simulations on this topic exist (Zhang et al., 2009; Li and Xu, 2017; Wutz et al., 2020; Shekhar and Jayanti, 2002; Sahu et al., 1999). On the one hand, numerical simulations offer the advantage that they can be in general carried out without major experimental effort, and thus usually much more cost-effectively. In addition, numerical simulations give a good overview of the mixing behavior of stirred tanks, as not only global mixing times are determined but also local instantaneous concentration profiles can be visualized. Nevertheless, such work results often in a comparison of the global mixing times, since this information is the simplest possibility for experimental validation (Shekhar and Jayanti, 2002; Li and Xu, 2017; Montante et al., 2005). While global mixing times are easily measured, local mixing effects are often only compared subjectively. Numerical simulations in particular offer the possibility of identifying poorly mixed areas and compartment formation in the reactor, but this is often not considered.

A local and detailed insight regarding the mixing behavior in dead zones is especially important to detect phenomena like step wise compartment formation (Manikowski et al., 1994; Vasconcelos et al., 1996; Szalai et al., 2004; Sieblist et al., 2011; Woziwodzki and Jędrzejczak, 2011).

This manuscript discusses a reliable method for a suitable determination of the local mixing degree of low viscous fluids in stirred tank reactors to determine the local mixing time. In addition, it is described how to distinguish experimentally between the macro, micro mixing time distribution and which advantages result from the differentiated analysis. This work benefits from the advantages of the decolorization method with bromothymol blue compared to other measurement techniques, while a high spatial and temporal resolution image recording system is used for a systematic local evaluation of the color change. Motivated by the deep insights that are available with this method, numerical simulations have been performed by means of the Lattice-Boltzmann code *M-Star CFD* to confirm the strong deviation in the local mixing time distribution. Finally, the experimental investigations of the local mixing time distribution are compared with the numerical simulation to show that the method described here can be applied not only to experimental mixing time videos but also to synthetic videos based on simulations. The application of the method to numerical simulations thus enables for the first time the experimental validation of numerical simulations, which is not limited to single instantaneous concentration distributions, but takes the temporal history of the mixing into account.

2. Theoretical principles

Due to the fact that different terms are used in the literature to describe the mixing time, the terms used in this paper will be first explained in detail. First of all, in this paper we distinguish between the global and local mixing time. The global mixing time represents the mixing time of the whole reactor. Thereby, the local mixing time is defined for the concentration in any given small volume element within the reactor. For the local mixing time distribution, a corresponding two-dimensional projection of the reactor is divided into individual cells and the respective mixing time is specified for each cell. Thus, the distinction between global and local mixing time is only a geometric differentiation, which depends only on the choice of the system boundaries. Whereby the distinction between macro, meso and micro mixing essentially

refers to the macroscopic, mesoscopic and microscopic flow structures.

In the following, the experimental and numerical method for determining the local mixing time distribution and the respective terms are explained in detail. The measurement of the local mixing time depends basically on the decolorization method first proposed by Fox and Gex (1956). The change in pH after the addition of a diluted acid or base can be measured by means of a pH sensitive tracer such as phenolphthalein or bromothymol blue. This has the advantage that not only the global mixing time can be measured, but also the hydrodynamics as well as flow patterns can be visualized (Ascanio, 2015; Rosseburg et al., 2018). However, the subjective determination of the discolored state is often cited as a frequent disadvantage compared to objective methods such as conductivity measurements (Ascanio, 2015). This disadvantage can be eliminated by using modern image acquisition techniques with high spatial and temporal resolution and subsequent automatic image evaluation. Kraume and Zehner (2001) have shown that the determined mixing time based on the decolorization method and the conductivity method agree well. For the comparison of the two measuring methods, the volumetric mixing ratio of the acid to the base is a very important influencing parameter (Godleski and Smith, 1962). The acid to base ratio has no significant influence on the measuring technique, since the addition of different amounts of HCl only changes the applied jump in conductivity. However, the mixing ratio does influence the decolorization.

According to Godleski and Smith (1962), the longest mixing time is obtained with a volumetric mixing ratio of X = 1:1 (acid: base). From a ratio greater than X = 2:1, the global mixing time remains constant. According to the authors, this is due to two main mixing effects, namely micro and macro mixing. The distinction between micro and macro mixing is used according to fluid dynamics definition of macroscopic convection and microscopic diffusion (Sommer, 2010). Whereas the meso mixing is often considered as an intermediate step between the macro and micro mixing. Furthermore, mixing is often understood as the achievement of a homogeneous state. However, the macroscopic mixing quality and the microscopic mixing quality have a different character and are therefore considered separately (Sommer, 2010).

The acid to base ratio in the decolorisation method can be used to distinguish between the determination of the macroscopic and microscopic mixing time. For better illustration, the exemplary mixing process of two substances A and B is shown in Fig. 1. On the left side in Fig. 1 the initial state for a decolorization experiment is visualized. At the beginning of each experiment, the homogeneous distribution of a base A is achieved (see Fig. 1a & d). For the upper row (see Fig. 1a), an acid B is added stoichiometrical and for the lower row (see Fig. 1b), twice the amount of an acid B is added. Due to the fact that the decolorization method is based on a color change, a complete decolorization for a 1:1 mixing ratio is only achieved when acid and base are homogeneously distributed on a microscopic scale, which is defined by the Batchelor scale (Batchelor, 1959). As soon as the instantaneous neutralization reaction has taken place on a microscopic scale, the color change occurs and marks the microscopic mixing time (see Fig. 1c). In summary, for an acid/base-ratio of 1:1, the acid has to be distributed totally homogeneously in the whole reactor to achieve neutralization (see Fig. 1c). In the case of an acid/base-ratio larger than 1:1, it is sufficient that at least one molecule of acid finds one molecule of base for neutralization and therefore the color change occurs earlier (see Fig. 1e). This does not mean necessarily, that in every fluid element a homogeneous distribution has been reached. Therefore, macro mixing can be stated as completed whereas micro mixing might be not finished (see Fig. 1e compared to Fig. 1f). In addition, the reproducibility of the experiments increases with growing acid to base ratio (Godleski and Smith, 1962). Finally, the mixing volumetric ratio of acid and base must be adapted to the problem to be investigated. The knowledge of the micro mixing time for example is important for the scale-up of processes with fast chemical reactions. Whereas, the macro mixing time is of interest for slower processes like the cultivation of CHO cells. Nevertheless, the decolorization method has the decisive advantage that compared to local conductivity measurements, the entire reactor can be observed, and thus be included in the evaluation. The most commonly used pH indicator for optical determination of the mixing time is phenolphthalein, which has the disadvantage that it only has one color change in the alkaline range. Therefore, it is extremely important to keep the acid to base ratio constant.

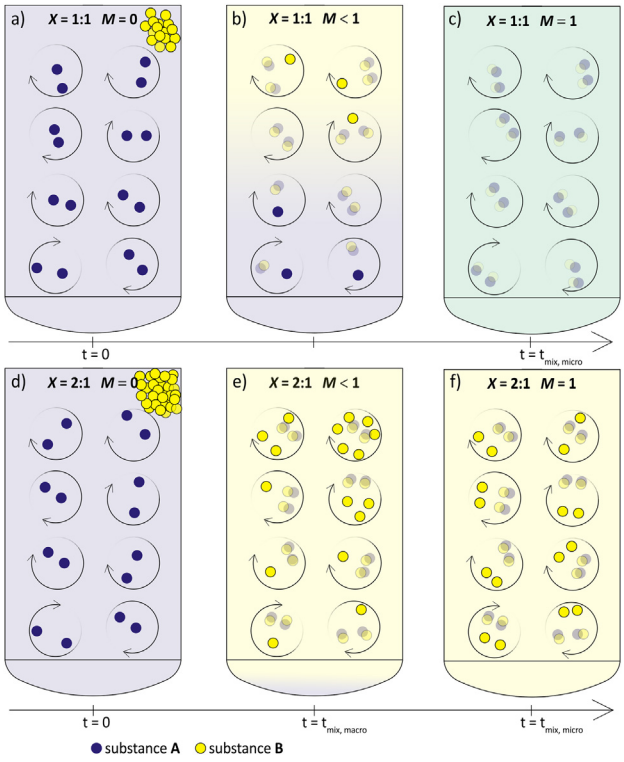

Fig. 1. Micro vs. macro mixing - Schematic representation of macro and micro mixing of two substances A and B with the same substance mixture (upper row) and a double excess of substance B (lower row); M: degree of homogeneity.

To investigate the local mixing time as well as the flow pattern, the use of a pH indicator with only one color change is not sufficient (Melton et al., 2002; Cabaret et al., 2007). For this purpose, a more differentiated pH indicator is required, such as bromothymol blue. Bromothymol blue has the great advantage that it shows further color changes in the neutral and acidic range (Alvarez et al., 2002; Melton et al., 2002; Lamberto et al., 1996). This means that considerably more information can be obtained in a computer-aided evaluation of the decolorization experiments. In particular, local undershoots in pH, which may occur during addition of diluted acid, can be displayed in this way.

2.1. Experimental method

In the following, the procedure for determining the local mixing time is described in detail. The method was validated using a 3 L glass reactor, allowing for an optimal control of the test conditions. The inner diameter of the stirred tank is $D = 130$ mm. The reactor is equipped with two standard Rushton stirrers with a diameter of $d = 36$ mm. The bottom distance s of the first stirrer is $s/d = 1$ and

the distance between the two stirrers is $s = 2d$. The working volume is $V_{\text{fill}} = 2.8\,\text{L}$, which corresponds to an aspect ratio of $H/D = 1.83$. The setup is shown in Fig. 2. Based on the recommendations of Zlokarnik (2001), the reactor is equipped with three baffles made of acrylic glass. The stirrer shaft is connected to the motor on the top of the reactor. The stirrer speed is regulated and controlled with a HiTec Zang ViscoPakt-X7.

For better optical observation, the reactor is immersed in a pool of water for refractive index matching. The diluted acid that induces the color change is added using a syringe pump (*type 11 Elite Infusion Only from* Harvard Apparatus). The point of addition (A) is located at a radius of $r_A = 50\,\text{mm}$ and an angle of 18° to the optical sensor. The addition was made 1 cm below the water surface. The diluted hydrochloric acid is added to the system via a 0.8 mm cannula and a nozzle outlet speed of 0.0895 m/s. Additionally, the pH and the conductivity are measured with a pH probe (*WTW SenTix© HW T 900* (accuracy ± 0,004 pH)) and a conductivity probe (*WTW TetraCon© 925–3* (accuracy 0.1% of the max. span)) respectively. The mixing process is recorded with a (*Nikon D7500*) camera and a (*Carl Zeiss ZF Planar f 1.4 50 mm*) lens. The videos were recorded at a frame rate of 60 Hz and a spatial HD (1080 × 1920) resolution of 235.3 μm/*px*.

At the beginning of each measurement, the pH is first set to pH = 7. Then 90 μ L of a 2 Molar NaOH solution is added to the system. The sodium hydroxide solution is dissolved at the operating parameters to be investigated. Subsequently the quantity of HCl required to neutralize the sodium hydroxide solution is added by using a syringe pump. As a signal to start the measurement, the background LED panel is switched on at the time of addition.

Fig. 3 shows the chronology of the decolorization experiment using the pH indicator bromothymol blue. For automated evaluation, a gray-scale image is calculated from the RGB images and an objective representation of the mixing processes is obtained by evaluating the gray value progression during the experiment for each point in the image. For this purpose, the average gray value

$$I_{\text{avg}}(t) = \frac{1}{N * M}\sum_{m=1}^{M}\sum_{n=1}^{N}(I(n,m,t) - I(n,m,t=0)) \tag{1}$$

is determined by means of averaging all pixels (n, m) of the reactor for each recorded time step. Where n and m indicate the respective pixel position in the image and N and M represent the maximum local resolution, which in this case corresponds to $N \times M = 1080 \times 1920$. The start value $I(n, m, t = 0)$ is subtracted from the gray value $I(n, m, t)$ to exclude those pixels that are not part of the reactor. The gray value profile $I_{\text{avg}}(t)$ will then be normalized to the final value so that the mixing process runs from 0 to 1

$$I_{\text{avg,norm}}(t) = \frac{I_{\text{avg}}(t)}{I_{\text{avg}}(t=\infty) - I_{\text{avg}}(t=0)} \tag{2}$$

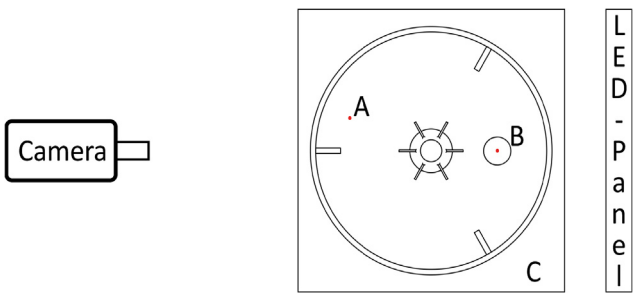

Fig. 2. Scheme of the experimental setup of the 3 L reactor (A: addition point; B: conductivity sensor; C: water basin)(top view).

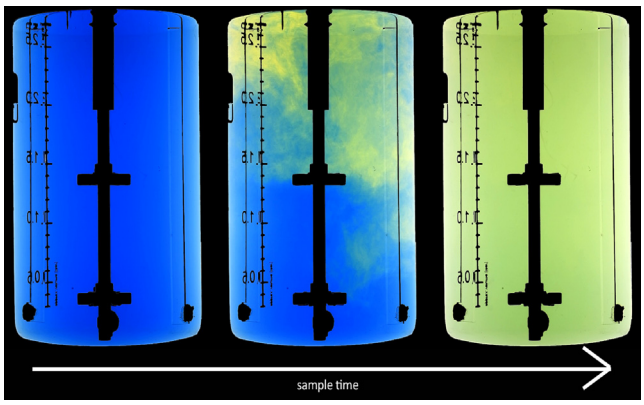

Fig. 3. Exemplary decolorization process with bromothymol blue at time t = 0; 15; 30 / s (masking around the stirring elements and baffle holder). (For interpretation of the references to colour in this figure legend, the reader is referred to the web version of this article.)

The mixing time criterion is set at 5% deviation of the final value, as it is often described in literature (Rosseburg et al., 2018).

$$t_{\text{mix},0.05} = t(I_{\text{avg,norm}}(t) = 1 \pm 0.05). \tag{3}$$

With this method, however, only the global mixing time can be evaluated objectively. The visual representation of the mixing process as well as the flow pattern remains only a subjective evaluation as long as the evaluation is not computer-aided. Often, this is represented by individual frames at certain points in time or as a time series of individual frames from the mixing process like in Fig. 3 or described in Alvarez et al. (2002), Cabaret et al. (2007), Sieblist et al. (2011).

It is important to note that the evaluation is based on a two-dimensional projection of the absorbed light by the pH indicator, so it is not possible to calculate back to the pH from the recorded images, except for stationary conditions. However, for simplicity, we must assume that the reactor is symmetrical. Therefore, it can be assumed that a two-dimensional projection is sufficient to represent the hydrodynamics with regard to the mixing time. This is definitely a strong limitation of the measurement method, due to the fact that, for example, very small deviations in the mixing time depending on the radius are averaged by the optical depth and thus underrepresented. Furthermore, it is not possible to distinguish whether observed structures are behind or in front of baffles. However, there are currently no possibilities to enable a three-dimensional back projection based on the method described here, which is why we will continue to work with the findings based on the two-dimensional projection, which provides the basis for further developments. In order to describe the hydrodynamics, it is necessary to look at either the progression of the mixing or the mixing on a local level. The local mixing also allows the quantification of compartments and the determination of concentration gradients occurring during the mixing process.

This enables both the global mixing time and the local mixing time to be determined. However, it requires a much higher computational power. For this purpose, the normalized gray value

$$I'_{\text{norm}}(n,m,t) = \frac{I(n,m,t)}{I(n,m,t=\infty) - I(n,m,t=0)} \tag{4}$$

for each pixel (n, m) is calculated for each point in time t. In addition, the temporal gradients for each pixel have to be preprocessed. For this purpose a LOWESS (locally weighted scatterplot smoothing) filter is used to calculate the smooth gray value. This procedure greatly reduces the measurement noise that might further disturb

the evaluation, especially for aerated conditions. Hence, the mixing time according to

$$t_{\mathrm{mix},0.05}(n,m) = t(I'_{\mathrm{norm}}(n,m,t) = 1 \pm 0.05) \tag{5}$$

can be calculated analogously for each pixel. In order to achieve a better comparison of different operating conditions with different global mixing times, the relative local mixing time distribution

$$t_{\mathrm{mix},0.05,\mathrm{rel.}}(n,m) = \frac{t_{\mathrm{mix},0.05}(n,m)}{t_{\mathrm{mix},0.05}} \tag{6}$$

can be calculated by relating the local mixing time distribution to the respective global mixing time $t_{\mathrm{mix},0.05}$. The formula states that the educts at a pixel are mixed if the gray value reaches the last time a deviation of 5% from the final value. Eventually, the calculated local mixing times can be displayed as pseudo-color image. Furthermore, the method can also be applied to numerical simulations. The numerical methods used in this study are described in detail below.

2.2. CFD method

The Lattice-Boltzmann (LB) approach is used to solve the transient Navier–Stokes equations. The commercial code *M-Star CFD 2.7.27* (*M-Star Simulations, LLC*) is applied. The applicability of the LB method and the governing equations have been discussed in the scientific literature (Eggels, 1996; Sungkorn et al., 2012; Derksen, 2001).

The static boundary conditions at the tank wall and the static installations are treated with a bounce-back routine (Smagorinsky, 1963) and the interactions between the fluid and the moving geometry (impellers) is handled with the immersed boundary method. The free surface has a free slip condition. The Lilly Smagorinsky LES (Large Eddy Simulation) closure model is used.

The discretization of space is done with a grid of points with a Lattice spacing $\triangle x = 5.2 \cdot 10^{-4}$ m which translates to ~ 21 million Lattice points. The time is solved explicitly so that a certain Courant Number C is satisfied to obtain the time step $\triangle t$:

$$C = u_{\max} \triangle t \triangle x^{-1} \tag{7}$$

The largest velocity $u_{\max}$ of the flow field is expected to be similar to the tip speed of the impeller which results in a time step of $\triangle t = 9.6 \cdot 10^{-5}$ s for a Courant Number of 0.1.

The tracers are implemented using the convection–diffusion equation:

$$\frac{\partial c}{\partial t} = \nabla \cdot (D \nabla c) - \nabla \cdot (u \cdot c) \tag{8}$$

where c is the concentration and $D = 9.31 * 10^{-9}\,\mathrm{m^2/s}$ (Cussler, 2009) is the diffusion coefficient.

A total of 90 s process time is simulated to ensure complete mixing of the tracer substance. The CFD simulation was performed on a desktop PC with a single NVIDIA Quadro RTX 8000. The simulation ran at a speed of 13.5 min wall time per second process time. The total simulated time of 90 s took 20 h elapsed real time. Here, the fluid dynamics used 21% of the numeric capacity, the scalar transport 30% and the immersed boundary (impeller) 18%. The full volumetric data were recorded every 0.1 s which consumed 18% of the simulation time.

The post processing is done with *ParaView 5.8.0*. First, the pH value is directly derived from the tracer concentration assuming complete dissociation according to

$$pH(t) = -\log_{10}(c_{\mathrm{i}}) \tag{9}$$

with the concentration

$$c_{\mathrm{i}} = c_{\mathrm{initial,i}} + X * c_{\mathrm{tracer,i}} \tag{10}$$

and the ratio factor

$$X = \frac{(c_{\mathrm{target,i}} - c_{\mathrm{initial,i}}) \cdot V_{\mathrm{fill}}}{c_{\mathrm{tracer,i}} \cdot V_{\mathrm{tracer}}}. \tag{11}$$

with the appropriate target concentration $c_{\mathrm{target,i}}$ to achieve the same pH as in the experiment. The tracer concentration for the neutralization reaction must be adjusted so that the factor $X = 1$. Thereby the tracer was added in the simulation at the same position as in the experiment by means of a square wave signal over 2 s.

Then the complete volume is rendered after mapping the pH value to the corresponding color spectrum of bromothymol blue. The corresponding color spectrum of bromothymol blue was experimentally recorded on the same experimental setup to ensure the best possible comparability between the simulation and the experiment. The transparency is adjusted to match the experimental pictures. For the evaluation of the rendered video, exactly the same evaluation algorithm has been used as for the experimental videos. There was no adaptation to the simulation.

3. Results and discussion

The new measuring and visualization procedure is discussed in the following on the basis of the described 3 L stirred tank reactor for one stirrer speed and different acid to base ratios. To validate the optical method, the global mixing time is compared with a local conductivity probe measurement technique. For the reactor shown in Fig. 3, the absolute local mixing time distribution is shown in Fig. 4 for a volumetric power input $P/V = 7.3\ \mathrm{W\ m^{-3}}$ (Power-Number Po=9), no aeration and an acid to base ratio of X = 1:1. For the local mixing time distribution shown in Fig. 4, the mixing time was also determined with a local conductivity probe, by means of the increase in salinity during the optical decolorization experiments. The mixing time of 44±11 s determined with the conductivity probe corresponds well with the average

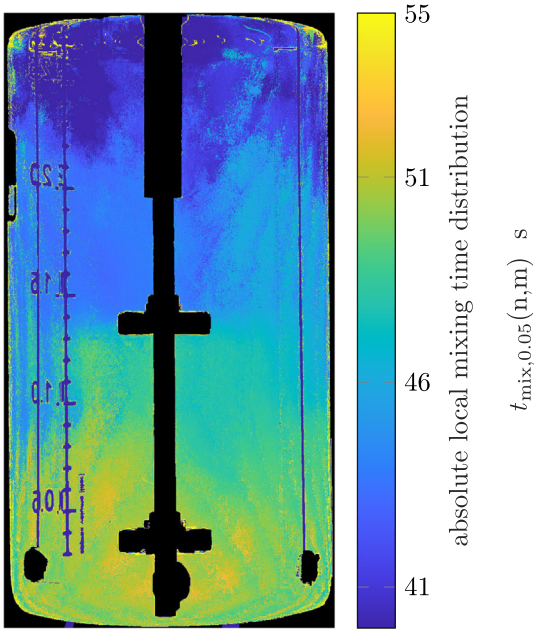

Fig. 4. Absolute local mixing time distribution by means of bromothymol blue and an acid to base ratio of X = 1:1 at $P/V = 7.3\,\mathrm{W\,m^{-3}}$, no aeration, $V_{\mathrm{fill}} = 2.8$ L, $t_{\mathrm{mix,global}} = 48.4$ s. (For interpretation of the references to colour in this figure legend, the reader is referred to the web version of this article.)

global mixing time of 47 ± 17 s shown in Fig. 4 (number of experiments $N_{exp.} = 14$). The deviation between the two measuring methods, as well as the high standard deviation, is due to the very small change in conductivity, as only very small amounts of diluted sodium hydroxide solution or hydrochloric acid are added for each test in order to neglect the influence on the viscosity. Based on the simulation, the mixing time of 35 s is comparable to the experimental data in the range of the experimental standard deviation. The special feature of the local mixing time distribution is that the formation of compartments can now be quantitatively resolved and visualized. Furthermore, a relative representation of the mixing time distribution has the advantage that a qualitative comparison of different states with each other is possible. Therefore, a comparison between the different mixing ratios of the acid to the base can be done. For this purpose, the relative mixing time distribution and the global mixing time (Eq. (3)) are calculated for different mixing ratios. In Fig. 5, the global mixing times are plotted against the mixing ratio and compared with the results from (Godleski and Smith, 1962) at similar specific power input. The deviations in the mixing time from the literature can be explained by the fact that a stirred tank reactor with strongly deviating geometry (aspect ratio H/D = 1, flat bottom, single Rushton, stirrer tip speed) was used. Additionally, the evaluation in the literature was done purely subjectively via the last color change. Nevertheless, a clear trend of decreasing global mixing time with increasing mixing ratio is visible, which is in good agreement to the presented results of this study. This behavior is confirmed by the relative mixing time distribution in Fig. 6, which shows four contour plots, each for one acid to base ratio respectively. Fig. 6 (left, first) shows that no clear compartments can be identified for the neutralization ratio of acid to base (1:1). It is not surprising that the relative mixing time distribution for a 1:1 ratio is much smoother compared to the other mixing ratios, since mixing for a 1:1 ratio not only requires the macroscopic distribution of the addition medium, but also micro and macroscopic homogeneity (see Fig. 1). On the other hand, with increasing acid to base ratios, convective transport processes dominate the mixing time, so that the relative mixing time distributions reflects the prevailing large-scale flow structures, which represent the macroscopic mixing. It is interesting to note that already from a surplus ratio of more than 1.25:1

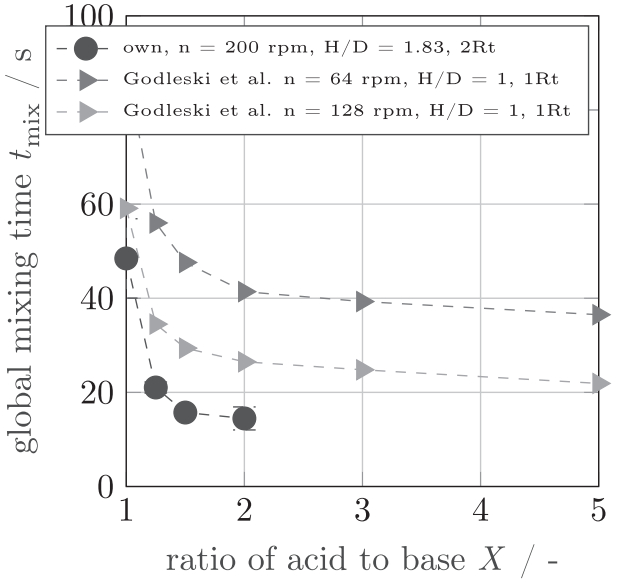

Fig. 5. Comparison of the global mixing time with data from the literature for different mixing ratios of acid to base.

clear compartments can be seen above the upper Rushton as well as between the two stirrers. The strong separation at the level of the upper Rushton turbine is likely caused by the radial flow, as visualized in Fig. 7. The lower Rushton turbine does not show this distinct separation because there is a stronger circulating component of the flow in the reactor bottom that moves partially below the baffles. Furthermore, there is a great similarity between the last two contour diagrams, although the global mixing time is not the same. This is further proof that a decolorization reaction with an excess of acid represents macroscopic mixing.

In addition, the representation of the local mixing times presented here offers a great possibility for the validation of CFD simulations of stirred tank reactors. For this purpose, the streamlines and the time-averaged flow profile for the reactor are shown in Fig. 7, which clearly shows the characteristic vortices of a Rushton turbine and the interaction of two Rushton turbines. Furthermore, a visual inspection of the time averaged data in Fig. 7 shows good agreement with the local mixing time distribution (Fig. 6, far right) and the resulting compartments. As already considered, the determination of the local mixing time distribution has the decisive advantage that it represents a new way of validating numerical simulation. Fig. 8 shows the experimental (left) and simulated (right) local mixing time distributions for the same geometry and the same operating parameters. The same color code is used for both illustrations in Fig. 8. The two illustrations are scaled equally. However, due to the perspective view and the refraction in the torispherical head, information near the wall and the bottom are missing in the experimental results, which is why the two illustrations do not have congruent dimensions. In general, the two illustrations match very good. Especially the bottom compartment and the dead zone in the upper right corner of the image are well reproduced by the simulation. Only the barrier between the upper and lower vortex of the upper Rushton is not appearing clearly in the simulation. This is probably due to the nature of the LES turbulence model. However, according to (Haringa et al., 2018) the simulated mixing times are in good agreement to the measured mixing times. But in the optical evaluation presented in this study we observe a slightly shorter global mixing time in the numerical simulation compared to the experiment. One reason for this is that the turbulent structures near the impeller and the trailing vortex are smaller and therefore the simulation averages the flow to a higher degree in these regions for a homogeneously spaced grid. This is most likely due to the fact that the barrier at the level of the top Rushton turbine, which can be observed reproducibly in the experiment, but is less pronounced in the simulation. In reality, this separation effect may be caused by the small turbulent structures within the trailing vortex. In the simulation, these smallest structures are modeled with the LES turbulence model and not fully resolved. By not resolving this barrier completely, the full separation capabilities are probably not given in the simulation. This may result in an artificially enhanced mass transport across the impeller plane where the turbulent structures act as a barrier between the region above and below the horizontal impeller plane in the optical mixing time experiment. This is also the reason why the global mixing time of the simulation is shorter than the experimentally determined mixing time. In essence, the obtained results show the importance of experimental validation for mixing time simulations, which of course is not always easy.

The enhanced analysis for determining local mixing time distributions based on the decolorization of bromothymol blue presented in this work offers completely new possibilities for process design and scale-up. Up to now, no objective methods for evaluating the local mixing as well as the flow pattern in stirred tank reactors except from the pLIF method are available. Further, laser-based measuring methods are usually limited to slim two-dimensional light sheets. Thereby, only certain areas of the system

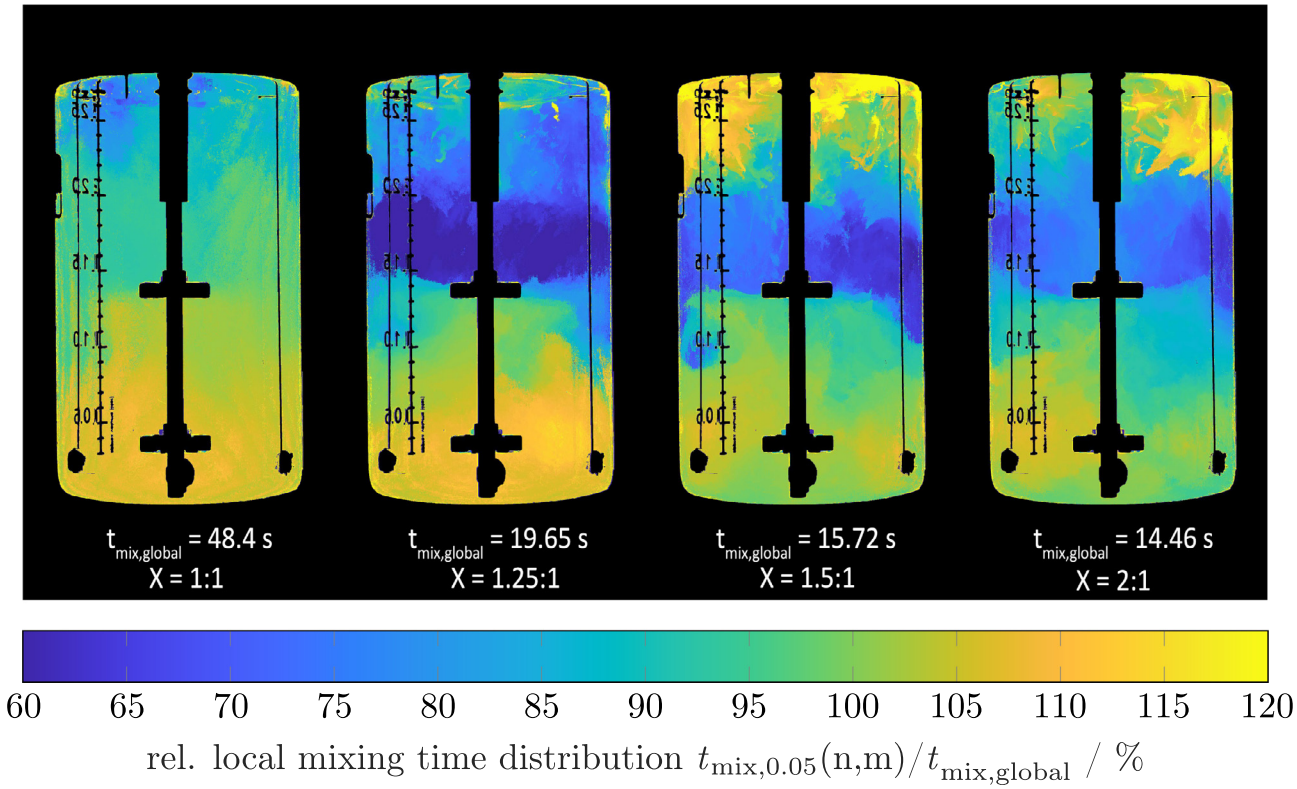

Fig. 6. Relative local mixing time distribution by means of bromothymol blue. (For interpretation of the references to colour in this figure legend, the reader is referred to the web version of this article.)

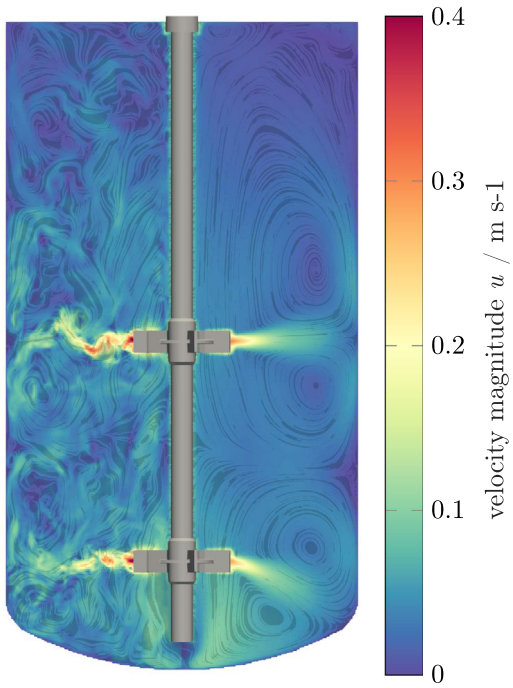

Fig. 7. Visualization of the simulated flow field at n = 200 rpm and no aeration (left part from stirrer: instantaneous streamlines, right part from stirrer: time averaged).

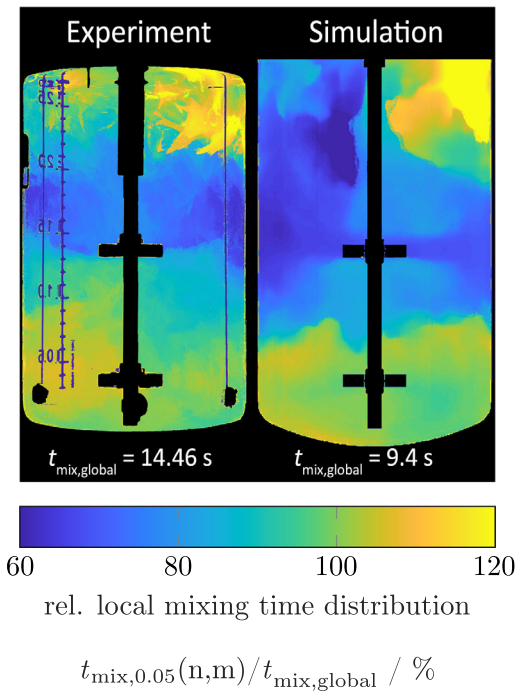

Fig. 8. Comparison of the local mixing time distribution for a double excess of HCl ($X = 2:1$), left: Experiment, right: Simulation.

can be observed and possible dead zones in the system might be overlooked. As a positive side-effect, the method presented in this study has the advantage that it is much cheaper and safer, because no expensive equipment is needed and no lasers have to be used. However, the optical access to the whole reactor volume is necessary. For this reason, the method cannot be applied to stainless steel reactors. A drawback compared to the PIV or pLIF method is that the hydrodynamic structures can only be derived on the basis

of a two-dimensional projection, so that the local mixing time distribution is the integral product over the reactor depth. However, for rotationally symmetrical problems, such as mixing in a stirred tank reactor, this is likely to be sufficient.

Additionally, it could be shown that compartments in the reactor due to stirrer placement can be detected. Especially poorly mixed areas in the system or dead zones can now be made visible. With this work it could be shown that the occurring undershoots in the pH, that cannot be distinguished with phenophtalein, can be detected with bromothymol blue. In addition, bromothymol blue can be used for a much more differentiated representation of the pH. In particular, this enables the distinction between micro and macro mixing. The proposed method has the decisive advantage that the measurement is non-invasive and follows the pH without any noticeable delay. This is especially important for very fast mixing processes and for processes that are faster than the response times of the sensors. Furthermore, it could be shown that the here presented method can also be used to validate simulation results.

The gained knowledge can significantly improve the understanding of the process. In this way, the local mixing time distribution can contribute to the improvement of future reactor geometries, e.g. preventing the formation of compartments by providing design parameters that can help to define optimal addition positions of the second educt in the future.

4. Summary

The here presented experimental method for the visualization of the local mixing time distribution represents a new way for the process characterization and validation of numerical simulations. It could be shown that the method is consistent, and thus provides a significantly higher information content compared to local probe measurement techniques for the determination of the mixing time. This is due to the fact that this method can not only be used to determine the global mixing time, but also to visualize and quantitatively describe the macroscopic flow structures. Besides the novel visualization of mixing processes, it could be shown that the method can also be applied for the evaluation of numerical simulations. This has been confirmed by numerical simulations of mixing in stirred tanks with the Lattice-Boltzmann code *M-Star CFD*. Both, experimental and numerical result shows a good agreement. Due to the low experimental effort, the method presented here can be applied to larger reactors, which is not trivial for other measurement techniques to measure the mixing time. For this reason, the method presented here will be implemented in a further step to the 15,000 L industrial scale stirred tank reactor made of acrylic glass which is available at the Institute of Multiphase Flows, Hamburg University of Technology.

Declaration of Competing Interest

The authors declare that they have no known competing financial interests or personal relationships that could have appeared to influence the work reported in this paper.

Acknowledgements

The authors gratefully express their gratitude to the company Boehringer Ingelheim Pharma GmbH & Co. KG for the financial support to conduct the presented research as well as all to all students involved who contributed to the success of this work. In particular we would like to thank our students Vincent Bernemann, Jakob Schulze and Helena Ostrinksy.

References

Alvarez, M.M., Arratia, P.E., Muzzio, F.J., 2002. Laminar mixing in eccentric stirred tank systems. Can. J. Chem. Eng. 80, 546.

Ascanio, G., 2015. Mixing time in stirred vessels: A review of experimental techniques. Chin. J. Chem. Eng. 23, 1065–1076. https://doi.org/10.1016/j.cjche.2014.10.022. http://www.sciencedirect.com/science/article/pii/S1004954115000877.

Aydin, Ö., Yapici, S., 2018. A novel method for the measurement of mixing time: A new application of electrochemical limiting diffusion current technique. Exp. Thermal Fluid Sci. 99, 242–250. https://doi.org/10.1016/j.expthermflusci.2018.08.002.

Batchelor, G.K., 1959. Small-scale variation of convected quantities like temperature in turbulent fluid part 1. general discussion and the case of small conductivity. J. Fluid Mech. 5, 113–133. https://doi.org/10.1017/S002211205900009X.

Bourne, J., 1983. Mixing on the molecular scale (micromixing). Chem. Eng. Sci. 38, 5–8. https://doi.org/10.1016/0009-2509(83)80129-8.

Buwa, V., Dewan, A., Nassar, A., Durst, F., 2006. Fluid dynamics and mixing of single-phase flow in a stirred vessel with a grid disc impeller: Experimental and numerical investigations. Chem. Eng. Sci. 61, 2815–2822. https://doi.org/10.1016/j.ces.2005.10.066.

Cabaret, F., Bonnot, S., Fradette, L., Tanguy, P.A., 2007. Mixing time analysis using colorimetric methods and image processing. Industr. Eng. Chem. Res. 46, 5032–5042. https://doi.org/10.1021/ie0613265.

Cheng, J., Feng, X., Cheng, D., Yang, C., 2012. Retrospect and Perspective of Micromixing Studies in Stirred Tanks. Chin. J. Chem. Eng. 20, 178–190. https://doi.org/10.1016/S1004-9541(12)60378-4.

Cussler, E.L., 2009. Diffusion: Mass Transfer in Fluid Systems. Cambridge Series in Chemical Engineering. Cambridge University Press. https://doi.org/10.1017/CBO9780511805134.

Danckwerts, P.V., 1952. The definition and measurement of some characteristics of mixtures. Appl. Scient. Res., Sect. A 3, 279–296. https://doi.org/10.1007/BF03184936.

Derksen, J., 2001. Assessment of large eddy simulations for agitated flows. Chemical Engineering Research and Design 79, 824–830. http://www.sciencedirect.com/science/article/pii/S0263876201721193, doi: 10.1205/02638760152721334. 4th International Symposium on Mixing in Industrial Processes.

Eggels, J.G., 1996. Direct and large-eddy simulation of turbulent fluid flow using the lattice-boltzmann scheme. Int. J. Heat Fluid Flow 17, 307–323. https://doi.org/10.1016/0142-727X(96)00044-6. http://www.sciencedirect.com/science/article/pii/0142727X96000446.

Fox, E.A., Gex, V.E., 1956. Single-phase blending of liquids. AIChE J. 2, 539.

Godleski, E.S., Smith, J.C., 1962. Power requirements and blend times in the agitation of pseudoplastic fluids. AIChE J. 8, 617.

Haringa, C., Vandewijer, R., Mudde, R.F., 2018. Inter-compartment interaction in multi-impeller mixing. part ii. experiments, sliding mesh and large eddy simulations. Chem. Eng. Res. Des. 136, 886–899. https://doi.org/10.1016/j.cherd.2018.06.007. http://www.sciencedirect.com/science/article/pii/S0263876218302922.

Hoogendoorn, C.J., den Hartog, A.P., 1967. Model studies on mixers in the viscous flow region. Chem. Eng. Sci. 22, 1689–1699. https://doi.org/10.1016/0009-2509(67)80204-5.

Kraume, M., Zehner, P., 2001. Experience with experimental standards for measurements of various parameters in stirred tanks: A comparative test. Chemical Engineering Research and Design 79, 811–818. http://www.sciencedirect.com/science/article/pii/S026387620172117X, doi: 10.1205/02638760152721316. 4th International Symposium on Mixing in Industrial Processes.

Lamberto, D., Muzzio, F., Swanson, P., Tonkovich, A., 1996. Using time-dependent RPM to enhance mixing in stirred vessels. Chem. Eng. Sci. 51, 733–741. https://doi.org/10.1016/0009-2509(95)00203-0.

Lamberto, D., Muzzio, F., Swanson, P., Tonkovich, A., 1996. Using time-dependent rpm to enhance mixing in stirred vessels. Chem. Eng. Sci. 51, 733–741. https://doi.org/10.1016/0009-2509(95)00203-0. http://www.sciencedirect.com/science/article/pii/0009250995002030.

Li, L., Xu, B., 2017. Cfd simulation of local and global mixing time in an agitated tank. Chin. J. Mech. Eng. 30, 118–126. https://doi.org/10.3901/CJME.2016.1107.129.

Manikowski, M., Bodemeier, S., Lübbert, A., Bujalski, W., Nienow, A.W., 1994. Measurement of gas and liquid flows in stirred tank reactors with multiple agitators. Canad. J. Chem. Eng. 72, 769–781. https://doi.org/10.1002/cjce.5450720502.

Manna, L., 1997. Comparison between physical and chemical methods for the measurement of mixing times. Chem. Eng. J. 67, 167–173. https://doi.org/10.1016/S1385-8947(97)00059-4.

Mao, Z., Yang, C., 2017. Micro-mixing in chemical reactors: A perspective. Chin. J. Chem. Eng. 25, 381–390. https://doi.org/10.1016/j.cjche.2016.09.012.

Melton, L.A., Lipp, C.W., Spradling, R.W., Paulson, K.A., 2002. Determination of mixing time through color changes. Chem. Eng. Commun. 189, 322.

Montante, G., Moštěk, M., Jahoda, M., Magelli, F., 2005. Cfd simulations and experimental validation of homogenisation curves and mixing time in stirred newtonian and pseudoplastic liquids. Chemical Engineering Science 60, 2427–2437. http://www.sciencedirect.com/science/article/pii/S0009250904009169, doi: 10.1016/j.ces.2004.11.020. 5th International Symposium on Mixing in Industrial Processes (ISMIP5).

Otomo, N., Bujalski, W., Nienow, A.W., Takahashi, K., 2003. A Novel Measurement Technique for Mixing Time in an Aerated Stirred Vessel. J. Chem. Eng. Japan 36, 66–74. https://doi.org/10.1252/jcej.36.66.

Paul, E.L., Atiemo-Obeng, V.A., Kresta, S.M. (Eds.), 2004. Handbook of Industrial Mixing: Science and Practice. Wiley-Interscience, Hoboken, NJ, USA.

Rewatkar, V., Joshi, J., 1991. Effect of Impeller Design on Liquid Phase Mixing in Mechanically Agitated Reactors. Chem. Eng. Commun. 102, 1–33. https://doi.org/10.1080/00986449108910846.

Rice, A.W., Toor, H.L., Manning, F.S., 1964. Scale of mixing in a stirred vessel. AIChE J. 10, 125–129. https://doi.org/10.1002/aic.690100133.

Rodriguez, G., Micheletti, M., Ducci, A., 2018. Macro- and micro-scale mixing in a shaken bioreactor for fluids of high viscosity. Chem. Eng. Res. Des. 132, 890–901. https://doi.org/10.1016/j.cherd.2018.01.018. http://www.sciencedirect.com/science/article/pii/S0263876218300200.

Rodriguez, G., Weheliye, W., Anderlei, T., Micheletti, M., Yianneskis, M., Ducci, A., 2013. Mixing time and kinetic energy measurements in a shaken cylindrical bioreactor. Chem. Eng. Res. Des. 91, 2084–2097. https://doi.org/10.1016/j.cherd.2013.03.005. mixing. http://www.sciencedirect.com/science/article/pii/S0263876213000956.

Rosseburg, A., Fitschen, J., Wutz, J., Wucherpfennig, T., Schlüter, M., 2018. Hydrodynamic inhomogeneities in large scale stirred tanks - influence on mixing time. Chem. Eng. Sci. 188, 208–220. https://doi.org/10.1016/j.ces.2018.05.008. http://www.sciencedirect.com/science/article/pii/S0009250918302999.

Sahu, A., Kumar, P., Patwardhan, A., Joshi, J., 1999. Cfd modelling and mixing in stirred tanks. Chem. Eng. Sci. 54, 2285–2293. https://doi.org/10.1016/S0009-2509(98)00334-0. http://www.sciencedirect.com/science/article/pii/S0009250998003340.

Schaepe, S., Kuprijanov, A., Sieblist, C., Jenzsch, M., Simutis, R., Lübbert, A., 2013. kLa of stirred tank bioreactors revisited. J. Biotechnol. 168, 576–583. https://doi.org/10.1016/j.jbiotec.2013.08.032.

Shekhar, S.M., Jayanti, S., 2002. Cfd study of power and mixing time for paddle mixing in unbaffled vessels. Chem. Eng. Res. Des., 80, 482–498. http://www.sciencedirect.com/science/article/pii/S0263876202722132, doi: 10.1205/026387602320224067. materials Processing.

Sieblist, C., Jenzsch, M., Pohlscheidt, M., Lübbert, A., 2011. Insights into large-scale cell-culture reactors: I. Liquid mixing and oxygen supply. Biotechnol. J. 6, 1532–1546. https://doi.org/10.1002/biot.201000408.

Smagorinsky, J., 1963. General circulation experiments with the primitive equations. Mon. Weather Rev. 91, 99–164. https://doi.org/10.1175/1520-0493(1963)091<0099:GCEWTP>2.3.CO;2.

Sommer, 2010. Micro and Macro Mixing - Analysis, Simulation and Numerical Calculation. In: chapter The Variance as Measured Variable for the Evaluation of a Mixing Process or for the Comparison of Mixtures and Mixers. Springer, Berlin, Heidelberg, pp. 2–16. https://doi.org/10.1007/978-3-642-04549-3.

Sungkorn, R., Derksen, J., Khinast, J., 2012. Modeling of aerated stirred tanks with shear-thinning power law liquids. Int. J. Heat Fluid Flow 36, 153–166. https://doi.org/10.1016/j.ijheatfluidflow.2012.04.006. http://www.sciencedirect.com/science/article/pii/S0142727X12000550.

Szalai, E., Arratia, P., Johnson, K., Muzzio, F., 2004. Mixing analysis in a tank stirred with Ekato Intermig impellers. Chem. Eng. Sci. 59, 3793–3805. https://doi.org/10.1016/j.ces.2003.12.033.

Vasconcelos, J.M.T., Barata, J.M., Alves, S.S., 1996. Transitional mixing in multiple-turbine agitated tanks. Chem. Eng. J. Biochem. Eng. J. 63, 53–58. https://doi.org/10.1016/0923-0467(95)03072-7.

Woziwodzki, S., Jędrzejczak, Ł., 2011. Effect of eccentricity on laminar mixing in vessel stirred by double turbine impellers. Chem. Eng. Res. Des. 89, 2268–2278. https://doi.org/10.1016/j.cherd.2011.04.004.

Wutz, J., Waterkotte, B., Heitmann, K., Wucherpfennig, T., 2020. Computational fluid dynamics (cfd) as a tool for industrial uf/df tank optimization. Biochem. Eng. J. 160, 107617. https://doi.org/10.1016/j.bej.2020.107617.

Zhang, Q., Yong, Y., Mao, Z.S., Yang, C., Zhao, C., 2009. Experimental determination and numerical simulation of mixing time in a gas-liquid stirred tank. Chem. Eng. Sci. 64, 2926–2933. https://doi.org/10.1016/j.ces.2009.03.030. http://www.sciencedirect.com/science/article/pii/S0009250909002127.

Zlokarnik, M., 2001. Stirring: Theory and Practice. Wiley-VCH, Weinheim; New York. OCLC: ocm46693210.